

SUPPORTING INFORMATION

Critical Role of Nanoinclusions in Silver Selenide as a Promising Room Temperature Thermoelectric Nanocomposites

*Khak Ho Lim,^a Ka Wai Wong,^b Yu Liu,^c Yu Zhang,^c Doris Cadavid,^d Andreu Cabot,^{*c,e} and Ka Ming Ng^{*a}*

^a. Khak Ho Lim, Prof. Ka Ming Ng
Department of Chemical and Biological Engineering, Hong Kong University of Science and Technology, Clear Water Bay Hong Kong

^b. Dr. Ka Wai Wong,
Genvida Technology Co. Ltd.

^c. Dr. Yu Liu, Yu Zhang, Prof. Andreu Cabot
Catalonia Energy Research Institute - IREC, Sant Adria de Besòs, 08930 Barcelona, Spain.

^d. Prof. Doris Cadavid,
Departamento de Física, Universidad Nacional de Colombia, 111321 Ciudad Universitaria, Bogotá, Colombia.

^e. ICREA, Pg. Lluis Companys 23, 08010 Barcelona, Spain

**E-mail:*

A. CABOT: *acabot@irec.cat*

Ka Ming NG: *kekmng@ust.hk*

Contents

| | |
|--|-----|
| 1. Chemical and synthesis..... | S3 |
| 2. EDS spectrum for Ag ₂ Se nanocrystals | S4 |
| 3. Particle size distribution of synthesized Ag ₂ Se | S5 |
| 4. SEM and EDX analysis of Ag ₂ Se pellets | S6 |
| 5. Table S1 Particle size calculated from XRD pattern | S7 |
| 6. TEM and elemental mapping of Te, Se, and Cu..... | S7 |
| 7. XRD pattern..... | S8 |
| 8. SEM and EDX analysis of 5 mol% Te/Ag ₂ Se nanocomposites | S9 |
| 9. SEM and elemental mapping of Te/Ag ₂ Se nanocomposites with different Te concentration | |
| 10. SEM and elemental mapping of Se/Ag ₂ Se and Cu/Ag ₂ Se nanocomposites..... | S11 |
| 11. Thermogravimetry analysis (TGA) of Ag ₂ Se, Te, Se, and Cu | S12 |
| 12. UPS spectrum of Ag ₂ Se..... | S13 |
| 13. Table S2 Work function for the Ag ₂ Se, Te, Se, and Cu | S13 |
| 14. Table S3 Hall effect measurement of Ag ₂ Se nanocomposites with different Te concentration..... | |
| 15. Table S4 Hall effect measurement of Ag ₂ Se nanocomposites with different nanoinclusions..... | |
| 16. Table S5 Literature comparison between bulk Ag ₂ Se | S15 |
| 17. TE performance comparison among different Ag ₂ Se nanocomposites | S17 |
| 18. Literature comparison of ZT _{avg} | S18 |
| 19. Reproducibility test on best-performing Te/ Ag ₂ Se nanocomposites..... | S19 |
| 20. References..... | S20 |

1. Chemical and synthesis

Materials

Selenium powder- 100 mesh (Se, $\geq 99.5\%$), copper (I) chloride (CuCl, $\geq 99.99\%$), and ammonium thiocyanate (NH₄SCN $\geq 97.5\%$), and oleylamine (OLA, 70 %) were obtained from Aldrich Chemical Co. Sodium borohydride (NaBH₄, $\geq 98.0\%$) and ethylene glycol (EG $\geq 99.8\%$) were purchased from Fisher. Analytical grade acetone, chloroform, hexane, and ethanol were obtained from Acros Organic. All chemicals were used as received.

Synthesis

Synthesis of Se nanorods: Se nanorods were prepared using a previously reported procedure.¹ Briefly, 0.5 g of Se powder and 0.6 g of NaBH₄ were dissolved in 400 mL of DI water at 30 °C. The brick red mixture was proceeded for 48 hours and then precipitated out by adding an excess amount of acetone as precipitant and left overnight. This step allows the amorphous Se colloid to form trigonal Se nanorods. The precipitate was further washed by repetitive centrifugation (3000 rpm for 5 min) and redispersion with DI water and acetone to remove all unreacted chemicals. Finally, Se nanorods were vacuum dried and stored in argon-filled glove box for further use.

Synthesis of Cu nanorods: Cu nanorods were formed by following previously reported procedures but with a prolonged reaction time.² Briefly, 4 mmol of CuCl and 12 mL of OLA were added into a 50 mL three-neck flask. The mixture was first degassed at room temperature for 15 min before a second degassed step at 100 °C for 20 min. Then, the mixture was flushed with N₂ and heated to 200 °C. The solution was reacted further for 1 h at 200 °C and cooled to room temperature. 2 mL of TOP was injected into the solution while stirring to prevent the oxidation of Cu nanorods. The product was further washed by repetitive centrifugation (3000 rpm for 5 min) and redispersion with hexane and acetone to remove all unreacted chemicals. Finally, Cu nanorods was vacuum dried and stored in an argon-filled glove box for further use.

2. EDS spectrum for Ag₂Se nanocrystals

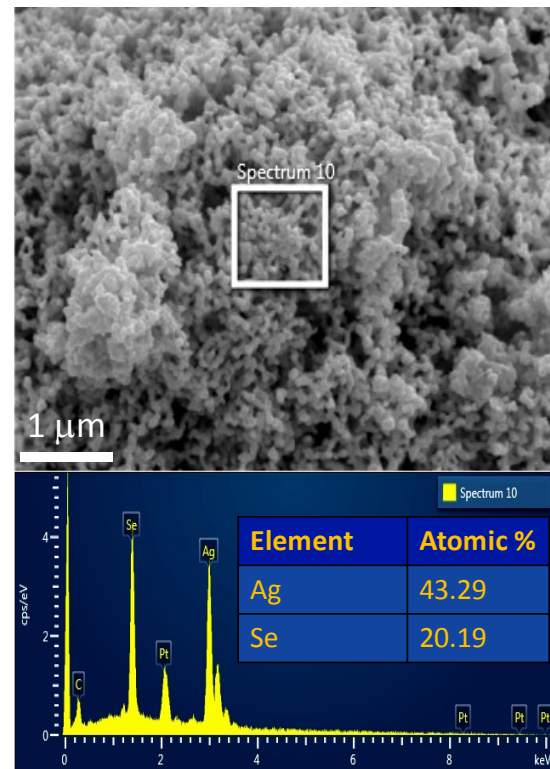


Fig. S1 Electron dispersive X-ray spectroscopy (EDX) obtained for Ag₂Se nanoparticles.

3. Particle size distribution of synthesized Ag₂Se

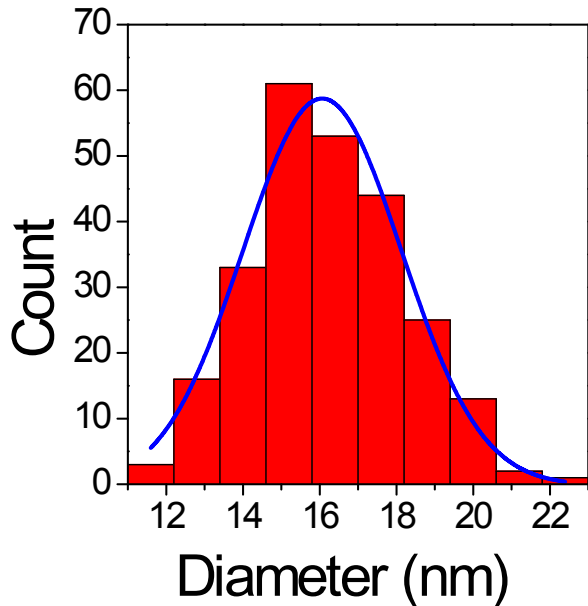


Fig. S2 Histogram showing particle size distribution of Ag₂Se nanocrystals as observed in TEM micrograph (Fig 1b), with a mean particle size of 16 nm. Whereas, the crystal size calculated from XRD pattern using Scherrer equation is approximately 17 nm.

4. SEM and EDX analysis of Ag₂Se pellets

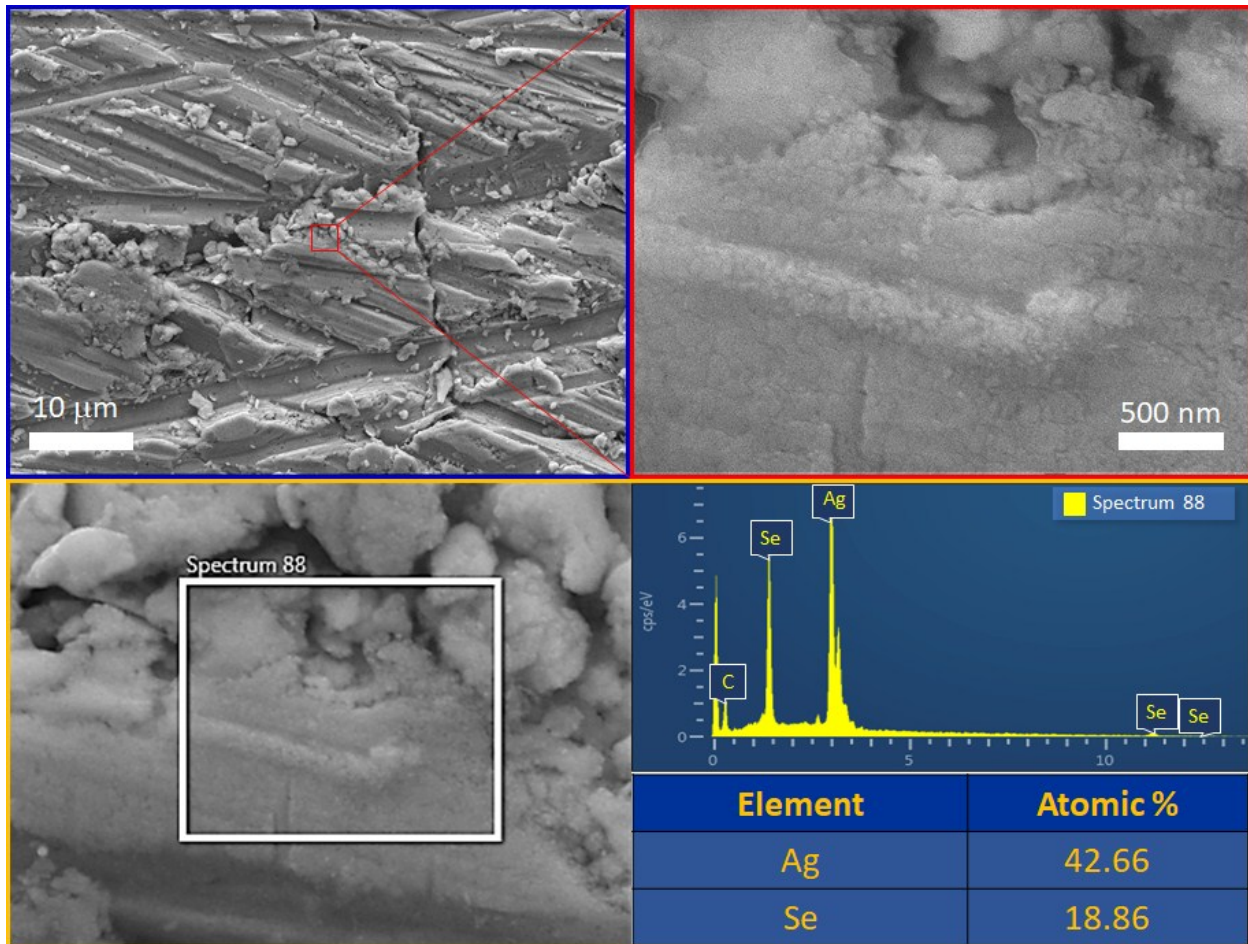


Fig. S3 Representative SEM micrograph of Te/Ag₂Se, the highlight area showing nanocrystals coalescences, with a crystal domain of ~ 32 nm, as calculated from XRD pattern using Scherrer equation (Table S1).

5. Table S1 Particle size calculated from XRD pattern

| Sample | Particle size [nm] |
|-----------------------------|-----------------------|
| Ag ₂ Se NCs | 17 |
| Ag ₂ Se (pellet) | 32 |
| 5 mol% Te | 28 |
| 7.5 mol% Te | 29 |
| 10 mol% Te | 29 |
| 20 mol% Te | 28 |
| 5 mol% Se | 25 |
| 5 mol% Cu | 29 |

6. TEM and elemental mapping of Te, Se, and Cu

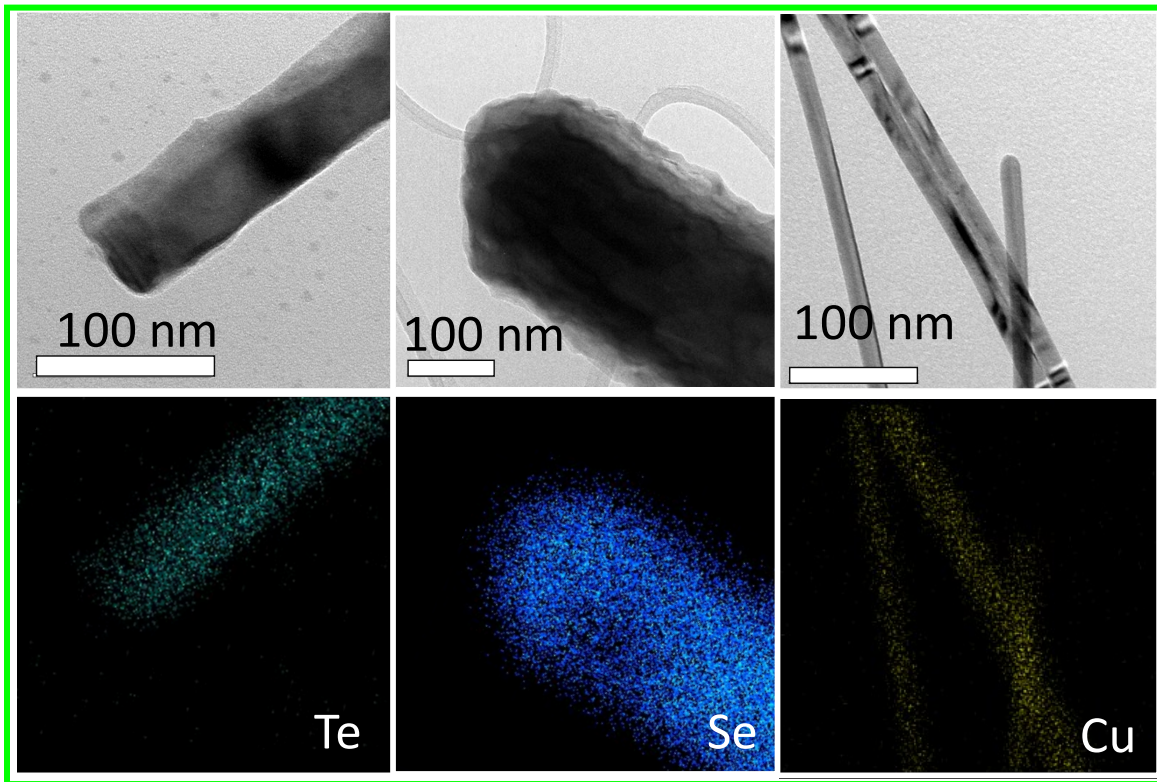


Fig. S4 Transmission electron microscope (TEM) micrograph and corresponded elemental mapping of Te, Se, and Cu nanorod.

7. XRD pattern

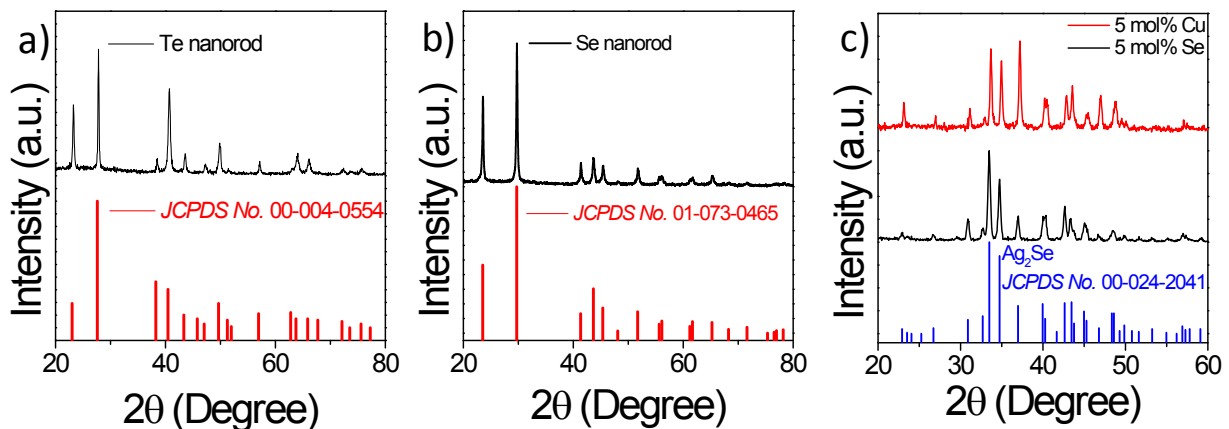


Fig. S5 X-ray diffraction (XRD) pattern of **a)** Te, **b)** Se, and **c)** Ag₂Se nanocomposites with 5 mol% Se (black line), and 5 mol% of Cu (red line).

8. SEM and EDX analysis of 5 mol% Te/Ag₂Se nanocomposites

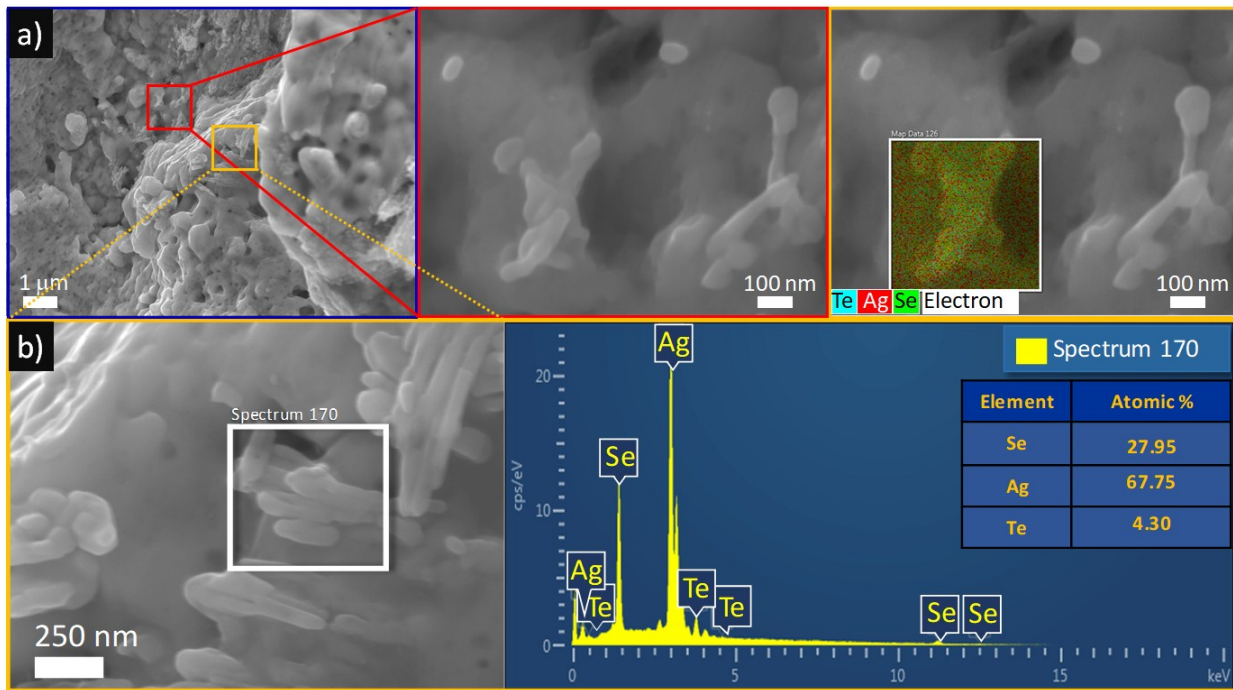


Fig. S6 **a)** Representative SEM micrograph and elemental mapping of Te/Ag₂Se nanocomposites with 5 mol% Te, and **b)** SEM and SEM-EDX spectrum of Te nanorods embedded within Ag₂Se matrix, which was found in the same sample.

The embedment of Te nanorod within Ag₂Se matrix was observed in Fig. S6, and further confirmed with EDX analysis.

9. SEM and elemental mapping of Te/Ag₂Se nanocomposites with different Te concentration

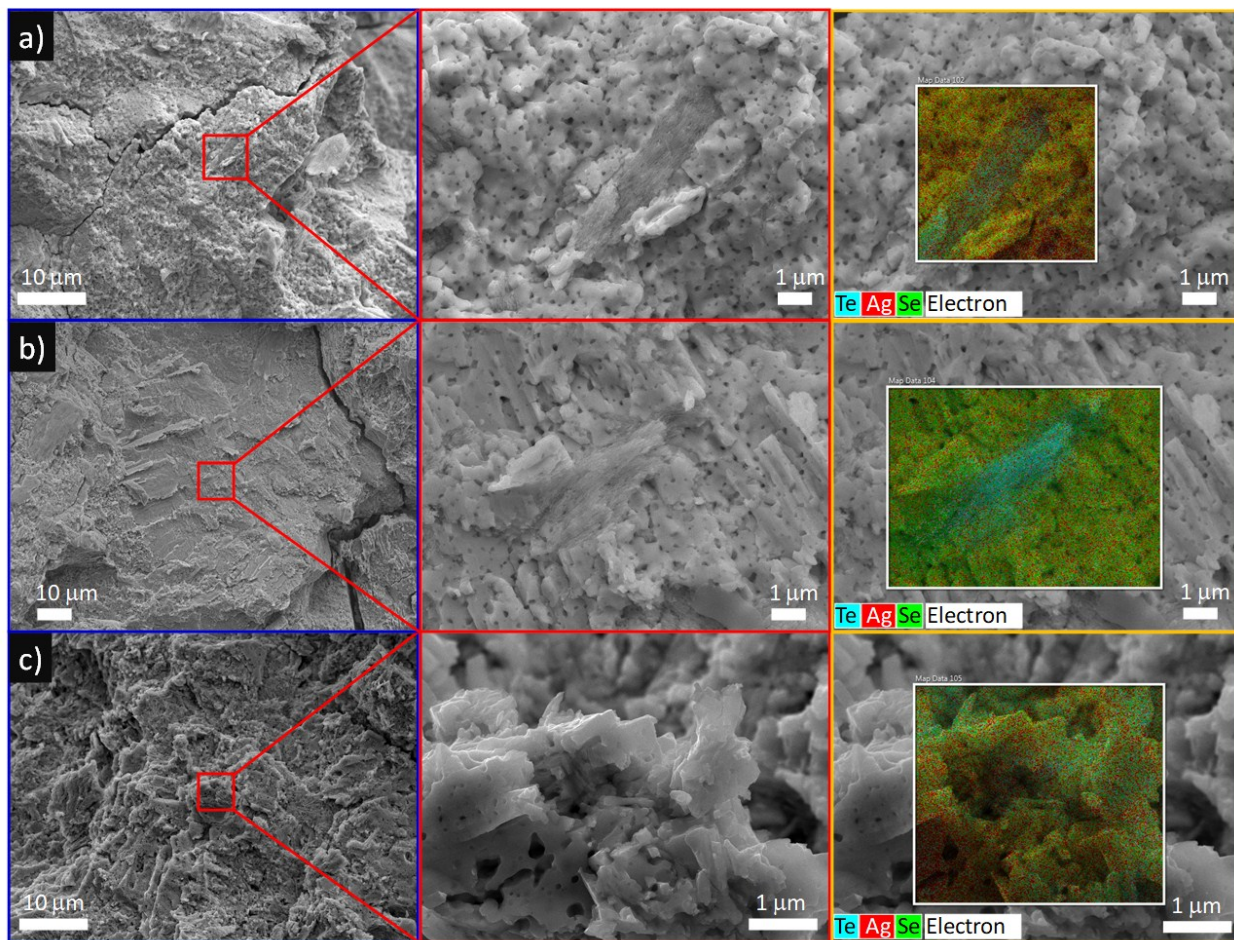


Fig. S7 Representative SEM micrograph of Ag₂Se nanocomposites with different Te concentration, where a) 7.5 mol%, b) 10.0 mol%, and c) 20.0 mol%.

10. SEM and elemental mapping of Se/Ag₂Se and Cu/Ag₂Se nanocomposites

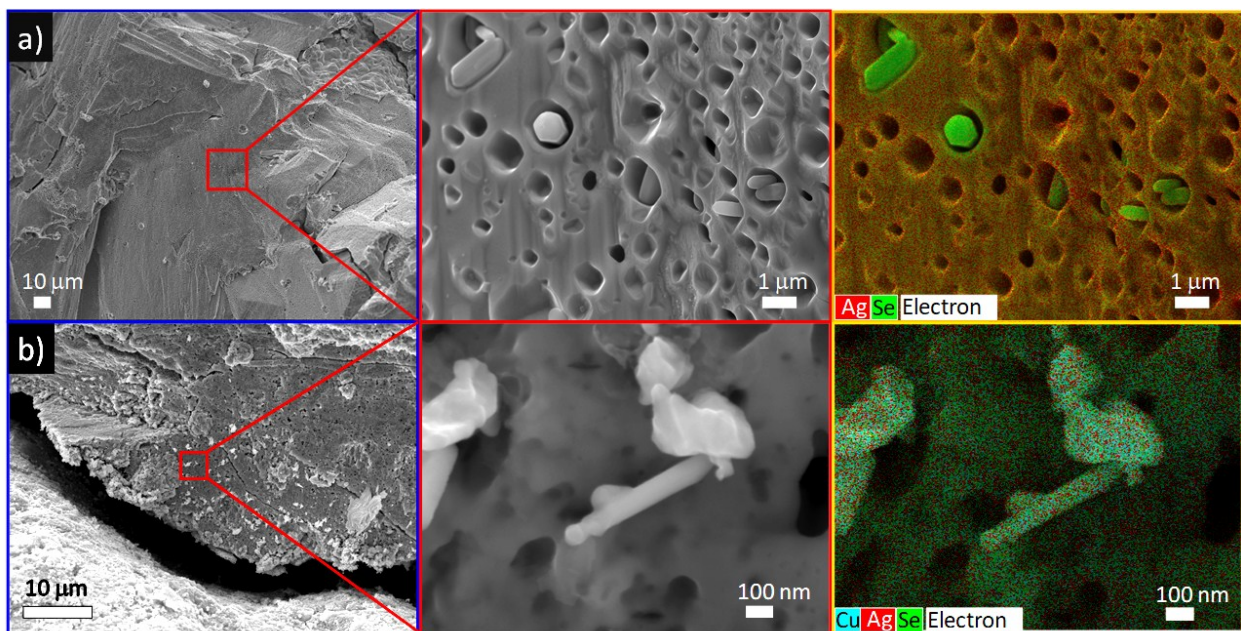


Fig. S8 Representative SEM micrograph of Ag₂Se nanocomposites, the highlight area showing the nanoinclusions are embedded in Ag₂Se matrix, with **a)** Se and **b)** Cu.

From the SEM micrographs (red box) shown in Fig S7 and Fig S8, Te/Se/Cu nanoinclusions can be seen embedded within Ag₂Se, which is also confirmed with EDX elemental mapping (yellow box).

11. Thermogravimetry analysis (TGA) of Ag₂Se, Te, Se, and Cu

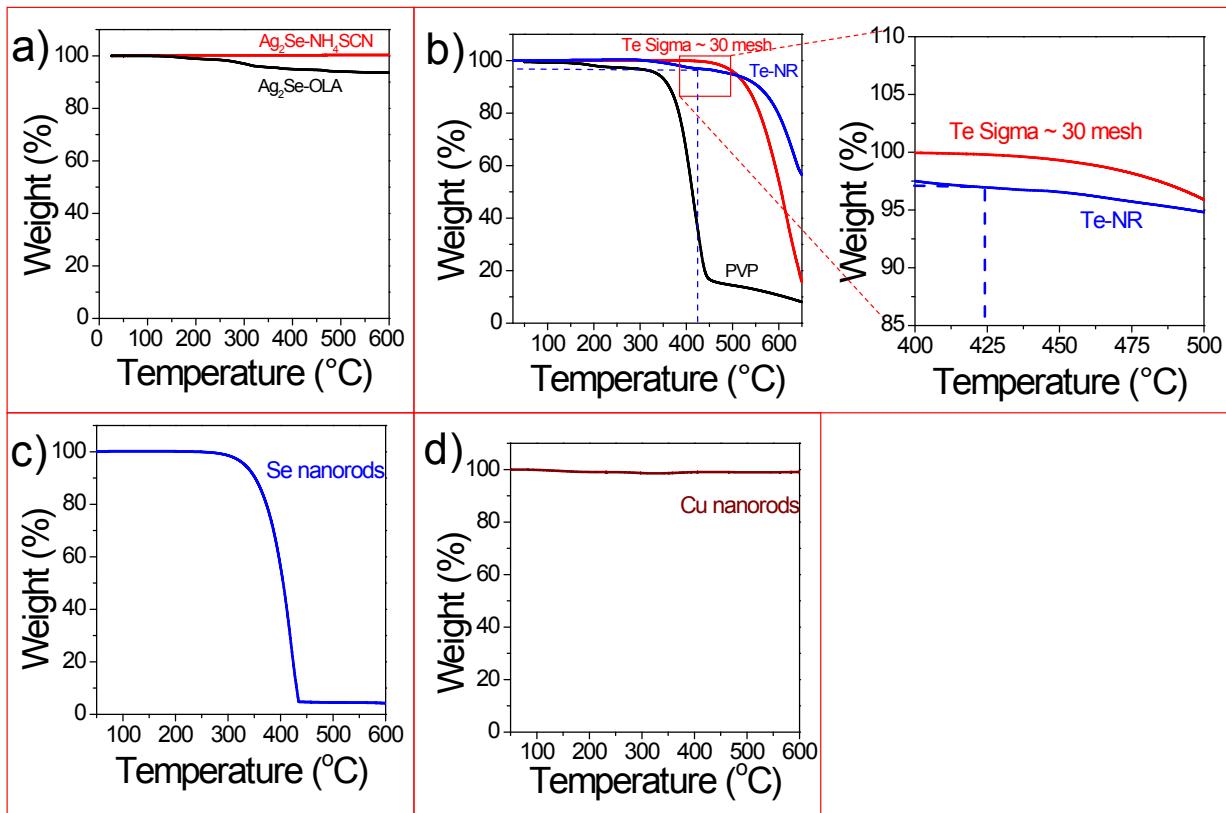


Fig. S9 TGA of **a)** Ag₂Se nanocrystals, **b)** PVP, Te nanorods synthesized (Te-NR) and Te powder (Sigma Aldrich), **c)** Se nanorods, and **d)** Cu nanorods.

As shown in **b)**, weight loss from 300-400 °C is due to decomposition of PVP, while in the enlarged diagram of **b)**, 400 °C onwards is attributed to the evaporation of Te, where the evaporation rate is usually affected by particle size. Meanwhile, Te, Se, and Cu showed high thermal stability, even up to 300 °C, showing good consistency with the previous report.³

12. UPS spectrum of Ag₂Se

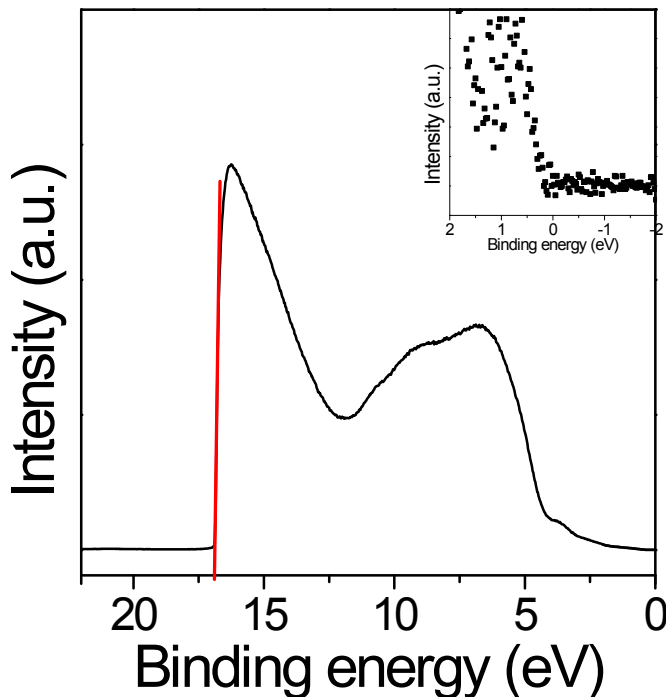


Fig. S10 Ultraviolet photoelectron spectroscopy UPS spectrum of Ag₂Se.

The work function, ϕ of Ag₂Se can be determined by subtracting the ultraviolet photon energy (He I) energy: 21.22 eV) and the binding energy cut off (~ 16.89 eV), thus $\phi_{\text{Ag}_2\text{Se}} = 4.33$ eV. Table S1 summarizes the ϕ value obtained from literatures and the UPS measurements.

13. Table S2 Work function for the Ag₂Se, Te, Se, and Cu

| <i>Element</i> | <i>Work function, ϕ literature [eV]</i> | ϕ <i>present work</i> [eV] |
|--------------------|---|---------------------------------|
| Ag ₂ Se | 4.30 ⁴ | 4.33 |
| Te | 4.95 ⁵ | 4.74 |
| Se | 5.90 ⁵ | 6.44 |
| Cu | 4.41-4.98 ^{5,6} | 4.28 |

14. Table S3 Hall effect measurement of Ag₂Se nanocomposites with different Te concentration

| (x mol%) Te/Ag ₂ Se | μ [cm ² V ⁻¹ s ⁻¹] | n [x 10 ¹⁸ cm ³] | R _H [cm ³ °C ⁻¹] |
|-----------------------------------|---|---|---|
| 0.0 | 323 | -11.4 | -0.55 |
| 5.0 | 625 | -7.37 | -0.85 |
| 7.5 | 807 | -6.99 | -0.98 |
| 10.0 | 900 | -5.00 | -1.25 |
| 20.0 | 953 | -3.60 | -1.73 |

15. Table S4 Hall effect measurement of Ag₂Se nanocomposites with different nanoinclusions

| (5 mol%) y/Ag ₂ Se | μ [cm ² V ⁻¹ s ⁻¹] | n [x 10 ¹⁸ cm ³] | R _H [cm ³ °C ⁻¹] |
|----------------------------------|---|---|---|
| Te | 625 | -7.37 | -0.85 |
| Se | 626 | -2.84 | -2.20 |
| Cu | 258 | -46.2 | -0.14 |

16. Table S5 Literature comparison between bulk Ag₂Se

| <i>Stoichiometry ratio</i> | <i>n</i> ($\times 10^{18}$) <i>cm³</i> | <i>ZT</i> | <i>Improvement (%)</i> | | <i>Synthesis/consolidation method</i> | <i>Year</i> |
|---|--|-----------|--|---|--|-------------|
| | | | $\frac{(ZT_{this\ work} - ZT_{previous})}{ZT_{previous}} \times 100\%$ | <i>%</i> | | |
| Ag _{1.9} Se _{1.1} | -5.50 | 0.479 | 66 | | Vibratory ball mill + SPS ⁷ | 2007 |
| Ag ₂ Se | -7.50 | 0.085 | 834 | | | |
| Ag _{2.025} Se _{0.975} | -16.0 | 0.268 | 196 | | | |
| Ag _{2.05} Se _{0.95} | -34.0 | 0.277 | 187 | | | |
| Ag _{2.1} Se _{0.9} | -57.5 | 0.195 | 307 | | | |
| Ag ₂ Se + 0.10 atomic% Ag | -9.10 | 0.069 | 1050 | | N.A. ⁸ | 2009 |
| Ag ₂ Se + 0.05 atomic% Ag | -8.30 | 0.539 | 47 | | | |
| Ag ₂ Se + 0.10 atomic% Se | -6.50 | 0.985 | -19 | | | |
| Ag ₂ Se + 0.05 atomic% Se | -7.10 | 0.840 | -5 | | | |
| Ag ₂ Se | - | 0.120 | 562 | Colloidal synthesis + hot press ⁹ | 2012 | |
| Ag ₂ Se | -7.83 | 0.630 | 26 | Solid solution + hot press (4h) ¹⁰ | 2013 | |
| Ag _{2.0006} Se | -5.56 | 0.630 | 26 | | | |
| Ag _{2.0027} Se | -4.97 | 0.480 | 65 | | | |
| Ag ₂ Se | -11.2 | 0.250 | 218 | Solid solution ¹⁰ | | |
| Ag _{2.0006} Se | -12.8 | 0.200 | 297 | | | |
| Ag _{2.0027} Se | -10.8 | 0.480 | 65 | | | |
| Ag ₂ Se | -7.49 | 0.593 | 34 | Solid solution + SPS ¹¹ | 2014 | |
| Ag ₂ Se _{1.08} | -5.65 | 0.637 | 25 | | | |
| Ag ₂ Se | - | 0.667 | 19 | Manual mixing + | 2016 | |

| | | | | SPS ¹² | |
|--------------------------------|-----------------------------------|-------|---|---|-------------------|
| Stoichiometry ratio | $n (\times 10^{18}) \text{ cm}^3$ | ZT | Improvement (%) $\frac{(ZT_{this\ work} - ZT_{previous})}{ZT_{previous}} \%$ | Synthesis method | Year |
| Ag ₂ Se | -5.09 | 0.700 | 13 | Manual mixing + cold press ¹³ | 2017 |
| Ag ₂ Se | -12.9 | 0.505 | 57 | Solid solution + SPS ¹³ | |
| Ag ₂ Se | -6.63 | 1.200 | -34 | Pulsed hybrid reactive magnetron sputtering ¹⁴ | 2018 ^a |
| Ag ₂ Se | -11.4 | 0.558 | 42 | Colloidal synthesis + hot press | (this work) |
| Ag ₂ Se + 5 mol% Te | -7.37 | 0.794 | | | |

17. TE performance comparison among different Ag₂Se nanocomposites

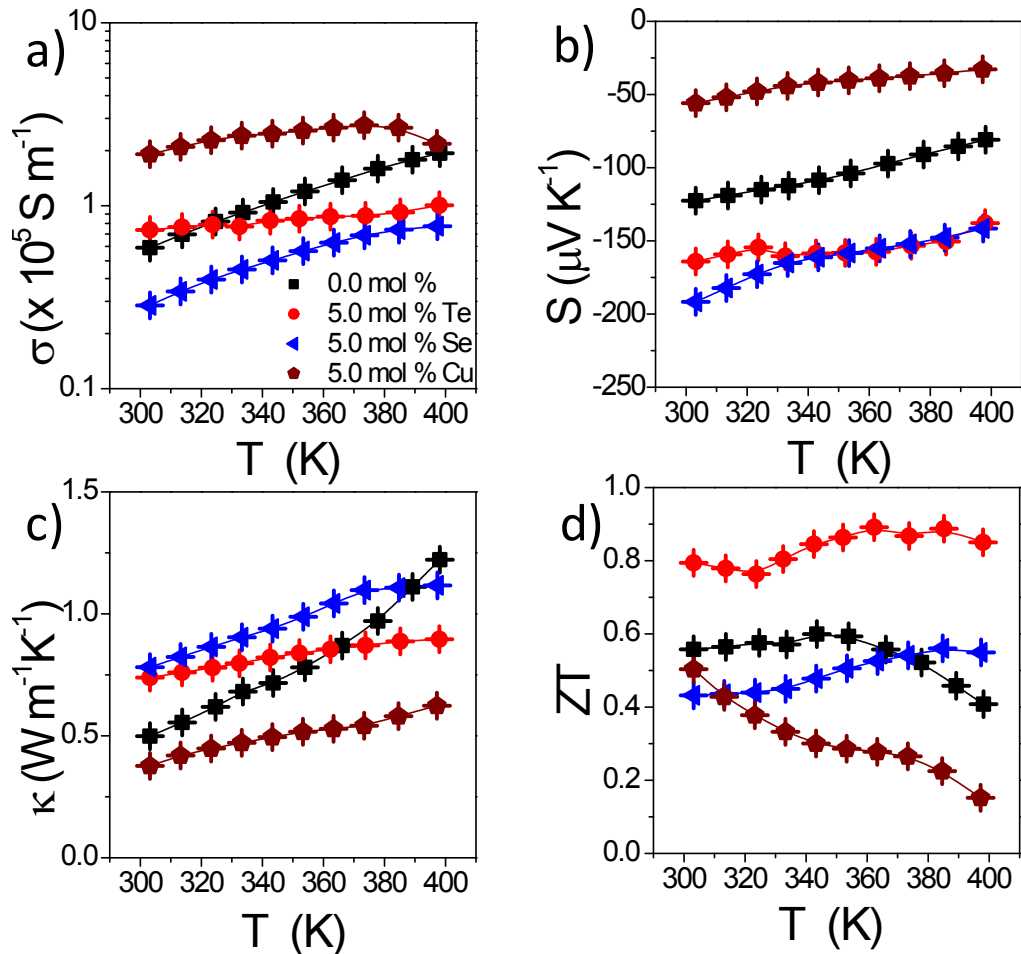


Fig. S11 Temperature dependence of **a)** electrical conductivity, σ , **b)** Seebeck coefficient, S, **c)** thermal conductivity, κ , and **d)** ZT of Ag₂Se nanocomposites, with 0.0 mol % (black square, ■), 5.0 mol% Te (red circle, ●), 5.0 mol% Se (left-blue triangle, ♦), and 5.0 mol% Cu (brown pentagon, ⊖).

18. Literature comparison of ZT_{avg}

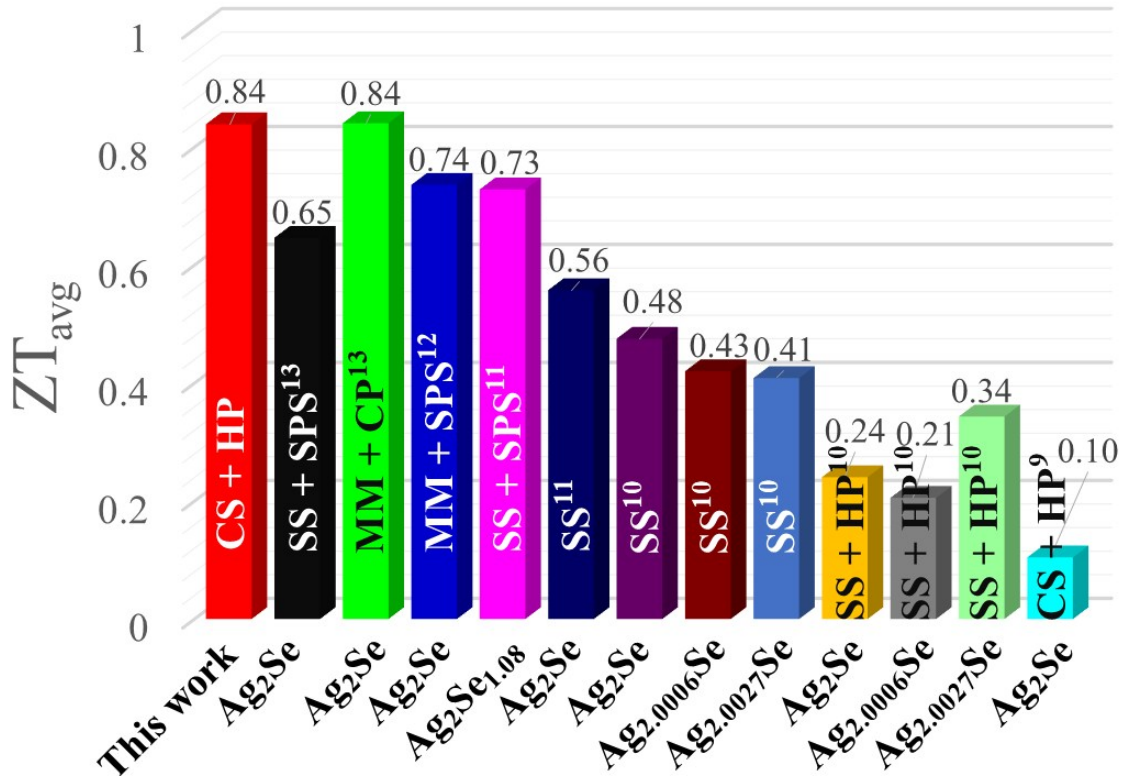


Fig. S12 Literature comparison of the average TE figures of merit (ZT_{avg}) for recently reported Ag₂Se, synthesized and consolidated by different method, *i.e.*, colloidal synthesis (CS), solid solution (SS), manual mixing (MM), hot press (HP), spark plasma sintering (SPS), cold press (CP).⁹⁻¹³

19. Reproducibility test on best-performing Te/Ag₂Se nanocomposites

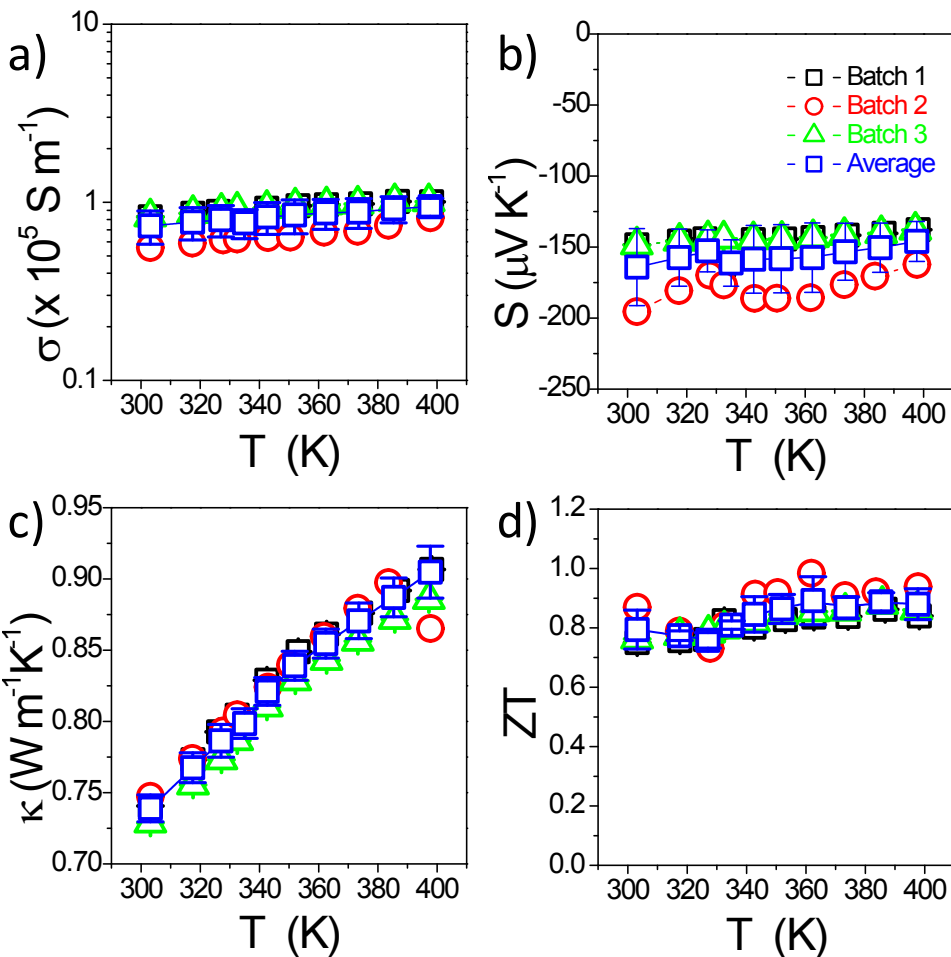


Fig. S13 Temperature dependence of **a)** electrical conductivity, σ , **b)** Seebeck coefficient, S , **c)** thermal conductivity, κ , and **d)** ZT of Te/Ag₂Se nanocomposites, for batch 1 (open-black square, \square), batch 2 (open-red circle, \circ), batch 3, (open-green triangle, \triangle), average (open-blue square, \square), with error bar.

20. References

- 1 U. K. Gautam, M. Nath and C. N. R. Rao, *J. Mater. Chem.*, 2003, **13**, 2845.
- 2 E. Ye, S. Y. Zhang, S. Liu and M. Y. Han, *Chem. - A Eur. J.*, 2011, **17**, 3074–3077.
- 3 D. A. Young, *Phase diagrams of the elements*, Lawrence Livermore National Laboratory, Livermore, CA (United States), 1975.
- 4 J. Qu, N. Goubet, C. Livache, B. Martinez, D. Amelot, C. Greboval, A. Chu, J. Ramade, H. Cruguel, S. Ithurria, M. G. Silly, E. Lhuillier, C. Gréboval and H. Cruguel, *J. Phys. Chem. C*, 2018, **122**, 18161–18167.
- 5 H. B. Michaelson, *J. Appl. Phys.*, 1977, **48**, 4729–4733.
- 6 M. Akbi and A. Lefort, *J. Phys. D. Appl. Phys.*, 1999, **31**, 1301–1308.
- 7 C. Lee, Y. H. Park and H. Hashimoto, *J. Appl. Phys.*, 2007, **101**, 0–5.
- 8 F. F. Aliev, M. B. Jafarov and V. I. Eminova, *Semiconductors*, 2009, **43**, 977–979.
- 9 C. Xiao, J. Xu, K. Li, J. Feng, J. Yang and Y. Xie, *J. Am. Chem. Soc.*, 2012, **134**, 4287–4293.
- 10 T. Day, F. Drymiotis, T. Zhang, D. Rhodes, X. Shi, L. Chen and G. J. Snyder, *J. Mater. Chem. C*, 2013, **1**, 7568.
- 11 W. Mi, P. Qiu, T. Zhang, Y. Lv, X. Shi and L. Chen, *Appl. Phys. Lett.*, 2014, **104**, 0–5.
- 12 H. Z. Duan, Y. L. Li, K. P. Zhao, P. F. Qiu, X. Shi and L. D. Chen, *JOM*, 2016, **68**, 2659–2665.
- 13 D. Yang, X. Su, F. Meng, S. Wang, Y. Yan, J. Yang, J. He, Q. Zhang, C. Uher, M. G. Kanatzidis and X. Tang, *J. Mater. Chem. A*, 2017, **5**, 23243–23251.
- 14 J. A. Perez-Taborda, O. Caballero-Calero, L. Vera-Londono, F. Briones and M. Martin-Gonzalez, *Adv. Energy Mater.*, 2018, **8**, 1–8.